Reconstruction of an ungauged flash flood event with large woody debris transport and its influence on hazard patterns.

Journal:	*Hydrological Processes*
Manuscript ID:	Draft
Wiley - Manuscript type:	Research Article
Date Submitted by the Author:	n/a
Complete List of Authors:	Ruiz-Villanueva, Virginia; Geological Survey of Spain (IGME), Geological Hazards division Bodoque, José M.; University of Castilla-La Mancha, Mining and Geological Engineering Department Díez-Herrero, Andrés; Geological Survey of Spain (IGME), Geological Hazard Division Eguibar, Miguel Ángel; Institute for Water and Environmental Engineering (IIAMA), Technical University of Valencia, Department of Hydraulic Engineering and Environment Pardo-Igúzquiza, Eulogio; Geological Survey of Spain (IGME), Research and Geoscientific Prospective Department
Keywords:	large woody debris, flood hazard analysis, ungauged basin, flash flood, clogging curves

Reconstruction of an ungauged flash flood event with large woody debris transport and its influence on hazard patterns.

V. Ruiz-Villanueva, J.M. Bodoque, A. Díez-Herrero, M. A. Eguibar, E. Pardo-Igúzquiza

ABSTRACT

An important flash flood accompanied by large quantities of woody material occurred in 1997 in Venero Claro (Sierra de Gredos, Central Spain), causing economic losses, and widespread geomorphologic changes The woody remnants formed temporary dams or clogged bridge sections, raising the water level upstream The main aim of this article is to reconstruct the 1997 event, analysing the influence of woody debris transport on the flood hazard pattern The peak discharge was estimated at 123 ± 18 m^3 s^{-1} (7.94 ± 1.16 m^3 s^{-1} km^{-2}) using empirical equations based on palaeohydraulic evidence. The reconstruction of the hydrological catchment response and the estimation of the amount of precipitation required to generate the peak discharge was carried out with a stochastic simulation of different rainfall field configurations and rainfall-runoff modelling.

Hydraulic simulation through an iterative process was used to reconstruct bridge obstruction to obtain the blockage or clogging curves. The percentage of bridge section obstruction occurring during the 1997 event was inferred as 48 ± 8 % and this was correlated with post-event observations and the estimated peak discharge upstream It was observed that the flooded areas were different from those where there was no wood. This conclusion helped to define the concept of equivalent return period, as the recurrence interval of an event of a certain where an obstruction is present, is equivalent

in depth and extension to an event without obstruction, but of greater magnitude. According to this concept, the magnitude of the event magnitude may be up to eight times greater as the obstruction increases. These results highlight the need to include obstruction phenomena in flood hazard analyses.

KEY WORDS: flash flood, flood hazard analysis, large woody debris, ungauged basin**,** mountain basin,

1. INTRODUCTION

The high potential risk associated with flash floods in mountain areas is due to a rapid and complex catchment response (Weingartner et al., 2003). Besides high water levels in the drainage network, important geomorphic changes as well as large transport of material (i.e. wood) must be considered as an additional factors.

Spatial and temporal scales of flash floods, combined with the space-time scales of conventional measurements of rainfall and discharge networks, make it particularly difficult to characterize these events properly (Borga et al., 2008; Marchi et al., 2009; Smith et al., 2011). Therefore, this type of flood phenomenon may therefore be poorly documented (in terms of data quantity and quality), particularly in mountainous areas (Sivapalan et al.,2003).

In addition to this, interaction between vegetation and geomorphological processes in forested mountain streams is heightened by abundant wood, high stream power and high sediment transport rates (Johnson et al., 2000). The effects of changing morphology during the event and the reduction of cross-sectional area due to transported material such as large wood may mean that risk analysis is not as reliable as expected.

The mobilization of woody material in rivers has been considered in the past, but very few studies have included this phenomenon in flood hazard and risk analyses (see Mazzorana et al., 2011 and references cited).

The reduction of cross-sectional area due to woody debris transport mentioned above can cause a quick succession of backwater effects with bed aggradation, flow diversions and local scouring processes, ultimately evolving toward embankment/bridge collapse and floodplain inundations (Diehl, 1997; Lyn et al., 2007; Comiti et al., 2008; Mao and Comiti, 2010). As a result, flooded areas are likely to be different from those predicted from models based on fixed-bed geometry in the absence of wood. The occurrence of bridge clogging or changing morphology can generally be predicted at least in qualitative terms by river managers, but current hazard maps do not take it into consideration. In an attempt to solve this issue Mazzorana et al., (2011) proposed a stochastic approach together with deterministic analysis to simulate reliable hazard pattern scenarios incorporating this process. This highlights the need to study these processes to reduce the uncertainties associated with stochastic models.

As a result, in ungauged forested mountain basins the reconstruction of this type of events will require particular attention to process interactions and their effects on critical stream configurations. For this reason, reconstruction of past events will provide a better understanding of the catchment response and will also improve hazard analysis.

In Spain, hydrometeorological networks mainly provide national daily data, but the most dangerous floods occur in a few hours. This may mean that the hydrologic response is measured with an inappropriate time interval (Camarasa and Tilford, 2002). As well as this limitation, the rain gauge network in the Spanish Central System is sparse and unevenly distributed, covering mainly valley and lowland areas. Flow gauges are mainly installed in large river basins, but even where they exist in smaller mountain

catchments, the flow time series may be wrongly recorded during extreme events, due to the damage often caused to gauges by the event itself or because discharge exceeds recordable levels.

This means that a lack of input data often implies a high level of uncertainty in the assessment of flood hazard and risk in ungauged mountain basins.

The Arroyo Cabrera catchment, one of hundreds of small ungauged forested mountain catchments in central Spain, is where an important flash flood occurred in 1997. The documentation of the flash flood reveals high peak flood discharges and a complex flood response. The main aim of this study, therefore, was to reconstruct this event, in terms of magnitude and also to understand the process interaction, particularly how the obstructive effect of wood at bridges affected the hazard. Three stages were defined to achieve this objective: (i) estimation of the flash flood water level and peak discharge; (ii) reconstruction of the hydrological catchment response and estimation of the rainfall required to generate the peak discharge, evaluating different rainfall field configurations; (iii) reconstruction of the clogging process. In addition, this paper attempts to answer the important question of how the large wood debris affects the magnitude of the event and the hazard patterns in general. To answer this question the clogging curves were designed and the concept of an equivalent return period was defined.

2. STUDY AREA AND THE FLASH FLOOD EVENT

2.1. The Arroyo Cabrera catchment

The study site is in the Arroyo Cabrera catchment, a torrential tributary of the Alberche River in the Tagus River Basin, on the northern slopes of the Sierra de Gredos, Spanish Central System (see Figure 1 A and B).

The catchment area is over 15.5 km^2 and is sub-triangular-circular in shape. The maximum difference in height within the watershed is 1188 m, and the main channel is 5500 m long, with an average slope of 21.6%. These characteristics are summarized in Table 1.

The bedrock consists of Upper Paleozoic granitoid covered by superficial Quaternary formations of conglomerates, gravels, sands and silts.

The local forest stand is formed predominantly by *Pinus pinaster* Ait., *Pinus sylvestris* L. *and Q. pyrenaica* Willd. In addition, riparian broadleaved species, *A. glutinosa* (L.), *F. angustifolia* (Vhal.) can be recognized in both river banks.

The continental Mediterranean climate of the study area is typical of Spanish medium mountain ranges. The mean annual temperature is 14.6 °C with 554 mm mean annual rainfall in the lower part and up to 2000 mm on the higher land (Palacios et al., 2011). Torrential rainfall events usually occur in autumn and winter, resulting in abundant surface runoff, sediment mobilization and related flash-flood events. The most important event identified to date was the 1997 flash flood. Figure 2 shows some of its effects.

Figure 1*: (A) Location of the study sitea within the Spanish Central System. (B) Arroyo Cabrera catchment. The forested area is shown in green. Raingauges and flow gauge*

are marked on the map. (C) Detail of the study reach, with sections described in the text (Section 2.2)

***Table 1**: Main physical characteristics of the Arroyo Cabrera catchment.*

2.2. The 1997 flash flood event: hydrogeomorphic descripction

The description of the hydrogeomorphic response is focused on specific sections due to their critical configuration. Critical configurations are understood here as spatial domains where torrential and fluvial processes have significant consequences in terms of risk.

The chronological description of the 1997 process can be summed up as follows: a complex sediment-laden flow was triggered by a shallow landslide (Ruiz-Villanueva et al., 2011); this evolved into a hyper-concentrated flow (Bodoque et al., accepted for publication). Section 1 shows the deposits and some toppled trees. When the flow had travelled 3.2 km downslope and most of the sediment transport was partially deposited, then avulsion took place in section 2 (Díez-Herrero, 2003). This process led to an important change in the drainage network pattern, and remobilized large quantities of sediment damaging the vegetation located within the stream and on the banks. The local newspapers described the event as an ecological catastrophe, with thousands of trees fallen.

Between sections 1 and 2 wood jams or individual pieces of wood deposited in the channel or riverside were not observed, although several toppled trees were seen lying transversal or oblique to the flow direction and many uprooted tree stumps.Along this reach the main recruitment was from processes on the upper slopes and the destabilizing action from the knock-on effect of the bedload transport.

Three small lobes were deposited upstream of the avulsion point. The secondary channel developed and travelled 1.3 km breaking away from the main channel after 160 m, with a maximum width of 35 m (between sections 3 and 4). While most of the solid material was deposited in the lobes or carried away by the main channel, most of the large woody debris (LWD) delivery was generated in the secondary channel.

The main channel travelled 1.4 km, with max. width 40 m, until it met the secondary channel again and they were reunited into a single channel 1 km upstream of the confluence with the Alberche River.

The section 3 is the Trampalones bridge, which was completely demolished by the deposition of a large wood jam deposit transversal to the flow direction. The volume of the wood jam is approx. 36 m^3 but most of the air pockets in the jam were filled with fine sediment or smooth woody debris. Between sections 3 and 4 approx. 400 m of a rural path were destroyed.

In section 5 (Figure 2A) evidence of the water level can be clearly seen (high water mark -HWM- in the small white building), with toppled and other damaged trees (scars were used as paleostage indicators –PSI-). The most important action in this section was the destruction of a small bridge across the river from the small building to the other side. Only the bridge abutments are still standing, and a gravel bar has developed upstream on the right bank. Some pieces, average length 6 m and average diameter 0.4 m, were deposited as usual in the LWD process, parallel to the flow direction and with the root system upstream. No wood jams developed here.

Finally, section 6 (Figure 2B) is the biggest obstacle in the stream, and the most critical section for flood hazard. Here important deposits of wood and boulders were observed, with some imbricate boulders lying on top of logs on the right bank. Some smooth woody debris was also found on top of the larger pieces.. Some of the logs are parallel

to the flow direction but others are transversal. The logs are of average length 7 m and average diameter c. 0.4 m. The volume on the right side of the bridge was estimated at 85 m^3, and most of this air volume was filled with sediment. The volume on the left side was c. 60 m^3. The evidence from observations, images and other indicators (e.g. fine sand and coarse wood deposits found on the bridge deck), show that the bridge was flooded due to the clogged wood.

Figure 2*: Images taken some days after the 1997 event. Picture A corresponds to Section 5, and B to Section 6 in figure 1.*

Some years after the 1997 flash flood event, this research team decided to monitor the Arroyo Cabrera watershed, installing 6 rain gauges (one per 2.5 km^2) and 1 stream gauge (Figure 1B). This later intensive monitoring of this small basin helped to assess its hydrological behaviour.

3. GENERAL METHODOLOGY

The methodology used to reconstruct the event has three main stages (Figure 3): 1. Estimating the order of magnitude of the event discharge using palaeoflood hydrology approaches. 2. Palaeohydraulic analysis. The aim was to estimate the peak discharge and its uncertainty, and to evaluate different scenarios to quantify the influence of the large woody debris on the flood magnitude, due to bridge clogging processes. 3. Reconstructing the hydrological response of the catchment combined with the stochastic simulation of the precipitation required for the estimated peak discharge.

The results were then validated using all the event information available, the systematic data recorded since 2004 and previous studies carried out in the area.

***Figure 3**: Methodological flowchart.*

4. PALAEOFLOOD DISCHARGE ESTIMATION

The 1997 event left evidence of the water surface elevation in various ways. As an example, the HWM visible on the small building located in the streamside (Figure 2A) as well as above the bridge deck (Figure 2B). Therefore, the first step was was to identify these HWM and PSI and survey them to estimate the water level in different sections. Then, a palaeohydrological approach was used to estimate the order of magnitude of the discharge and flow velocity due to the large accumulation of boulders transported during the event (Figure 2B). The mean flow velocity needed to transport this material was estimated using the range of boulder sizes, applying empirical methods (Costa, 1983; Baker et al., 1984; Johnson and Warburton, 2002; Kehew et al., 2010) this then allowed a range of discharges to be obtained (using the cross-sectional area).

According to the HWM the water depth upstream section 6 was ~7 meters, just 5 cm above the bridge deck. The same procedure was carried out for section 5, using the HWM observed on the small building and PSI scars on two trees the water level upstream this section was ~ 3 m (HWM_{S6}= 7.1m; HWM_{S5}= 2.4m; PSI_1= 2.8m;PSI_2= 3.2m).

The mean boulder size ranges from 400 to 600 mm Using an empirical approach (Costa, 1983) the flow velocity required to transport this type of material ranges from 3-4 m s^{-1},

using the cross sectional area (section 6, 35 m^2) the discharge range is estimated in the bridge section at 105-140 $m^3 s^{-1}$.

In a previous article (Ballesteros et al., 2011) the discharge of this event was estimated in the reach a few meters downstream of the bridge. They estimated 145 $m^3 s^{-1}$ as the minimum peak discharge for which all scars are submerged.. Then, they established a peak discharge of 79 ± 14 $m^3 s^{-1}$. These values are calculated for a different reach (several meters downstream the bridge, therefore influence for its lamination) but agree with our results.

5. HYDROMETEOROLOGICAL RECONSTRUCTION

5.2. Spatial rainfall field configuration

Only 10 daily raingauges were recording data on December 1997 in Sierra de Gredos (recorded data of the event are shown in Figure 4). They were located within a radius of 80 km, with most of them installed at low altitudes.

Where the precipitation data network does not have rain gauges located at high elevations, the main risk is underestimation of precipitation values at higher points (Vélez et al., 2007). Therefore, simulations are needed to model stochastic behaviour of the climatic system .It is also advisable to use secondary information from an easy-to-measure variable, with complete coverage of the study area and correlated with rainfall, such as altitude obtained through a digital elevation model (DEM). The advantage has been shown of using the DEM together with rain gauge data to estimate daily rainfall (Pardo-Igúzquiza, 1998; Goovaerts, 2000).

Stochastic simulation of these daily data from the 10 stations provided a description and a measure of uncertainty of the spatial variability of this phenomenon. This was done by

generating multiple realizations (500) of the stochastic process modelling the spatial distribution under study. All the simulation tools implemented belong to the sequential simulation category using the Stanford Geostatistical Modeling Software (SGeMS, Remy et al., 2009), and the *COSGSIM* algorithm which allows a co-kriging solving system to be chosen.

This algorithm simulates a Gaussian variable accounting for secondary information assuming that the variable is Gaussian (using a normal score transform to turn the variable values into a set of values that follow a normal standard distribution).

Let Z1(u) and Z2(u) be two correlated random variables. In this case, Z1(u) called the primary variable, is the daily rainfall data; and Z2(u) called the secondary variable, is the altitude; a digital elevation model (DEM) of 100 m pixel size was used. Then, it is necessary to transform Z1 and Z2 into Gaussian variables before the simulation, and they will be backtransformed to match the histogram of the actual values afterwards. This backtransformation involves extrapolation in the tails of the distribution, for which the user has to set minimum and maximum allowed limits for the backtransformed values. The Gaussian variogram model chosen was exponential as usual in rainfall simulations (Grimes and Pardo-Igúzquiza, 2010) with no nugget effect and sill equal to 1. The variogram range was 46200 m.

Previous work in the study area (Ruiz-Villanueva et al., 2011) established an intensity-duration precipitation threshold for triggering shallow landslides like the one in 1997. According to this study the critical rainfall amounts ranged from 215 - 324 mm depending on the storm duration (6-24h).

The realizations that met this imposed condition (minimum precipitation 215 mm and maximum precipitation 325 mm) and were representative of the known orographic

pattern of rainfall usual in this area, were assumed to be the most reliable and were selected for further evaluation.

Figure 4: *Example of stochastic realization which fulfilled the conditions so is reliable for use in hydrological simulation. Daily registered data is placed over the station (blue squares).*

Of the 500 computed stochastic simulations, 70 fulfilled the conditions imposed in the study, and 58 of these agreed with the regional orographic pattern. The spatial representation of one of these reliable simulations is shown in Figure 4.

5.2. Rainfall-runoff analyses

The intensive monitoring of this small basin since 2004, with 6 rain gauges and one flow gauge, together together with an in-depth knowledge of the landscape and geomorphic structure of the area, allowed calibration and validation of the hydrological simulation.

A calibrated rainfall–runoff model was developed using HEC-HMS 3.5 (USACE, 2010a) to estimate modern flood discharges in the Arroyo Cabrera catchment.

The basin model was designed using HEC-GeoHMS 4.2 (USACE, 2009). The degree of detail of the stream network was defined by taking into account a 1% of the total drainage area as the upstream drainage area threshold (in square units). The basin model consists of 9 subbasins. This disaggregation was based on the spatial distribution including the physiographic factors determining a homogenous hydrologic response (i.e., lithology, cover type and hydrologic condition, slope, etc.).

The transformation of excess precipitation to runoff was carried out using the SCS dimensionless unit hydrograph method. The antecedent condition was established as wet based on the cumulated precipitation in previous days (Ruiz-Villanueva et al., 2011). Channel routing was simulated implementing the Muskinghum-Cunge method. For baseflow, the recession method was implemented.

Calibration and validation of the hydrological model was limited by the short time series, with records for only 7 years. An automatic calibration routine was used for this where the sum squared residuals and univariate method were used as objective function and search algorithm, respectively.

Hydrological model calibration and verification were performed for selected recorded events exceeding a depth of 1 meter. The results show a good fit between simulated and observed peak discharges, with a Nash–Sutcliffe efficiency equal to 0.73 and correlation coefficient of 0.79.

Once the model had been calibrated, the inverse hydrological problem was solved to identify the rainfall field configuration for the 1997 event.

Several scenarios were simulated and the basin response was analysed to different design hyetographs resulting from the desegregation of the reliable stochastic realizations. These 15 minute time interval hyetographs were obtained by desegregating daily data using the available intensity-duration curves for Spain (Salas and Fernández, 2007), three hyetotypes and three storm durations (6, 12 and 24 h). These hyetotypes (Montescarchio et al., 2009) were: (A) triangular increasing rate hyetograph; (B) triangular decreasing hyetograph; (C) isosceles triangular hyetograph.

Therefore, 432 independent stochastic simulations were performed for all the combination of hyetotypes and rainfall volume. The spatially distributed daily rainfall including the orographic effect was obtained in this way.

A summary of the methods above from stochastic simulations to rainfall-runoff modelling is shown in Table 2.

***Table 2**: Summary of methods used in the Hydrometeorological reconstruction*

As a result of these simulations, and as expected, several different basin responses were observed: (i) for the three storm durations the lowest discharges were obtained with hyetotype B and the highest values obtained when type A was applied (59-73 % bias), whereas types C and A were very similar (8-25 % bias); (ii) the 6 h storm resulted in the highest discharges, with mean values ranging from 92 to 228 m^3/s depending on the hyetotype. Mean values for the 12 h storm ranged from 33 to 121 m^3/s and for the 24 h storm from 12 to 43 m^3/s; (iii) the scenarios that best reproduced the estimated peak discharge for the 1997 event were hyetotypes C and A for the 12h storm, and hyetotype B for the 6 h storm; based on the knowledge of the rainfall in the area, the most reliable are C and A.

The mean precipitation in the catchment from the selected scenarios was used to extrapolate from recent rainfall amounts (recorded within the catchment) to the amount of rainfall needed to produce a discharge of 123 $m^3\ s^{-1}$ downstream (an example of this is presented in the Figure 5).

***Figure 5:** Ratio (solid line) between a given volume of mean precipitation in the catchment of given duration (12h) and the discharge generated. Red dots are storm events from 2004-2011 correlated with observed discharges. Black triangles and grey squares are design storms and corresponding simulated discharges.*

Figure 5 shows that the mean precipitation in the catchment giving the estimated discharges ranges from 205 to 260 mm (233 ± 27 mm) for a 12h storm and using triangular increasing rate and isosceles triangular rate hyetographs, with simulated maximum rainfall intensities ranges from 25 to 4 mm/h. These results agree (in storm duration, amounts and intensities) with previous estimates based on landslide-triggering precipitation thresholds in 1997 (Ruiz-Villanueva et al., 2011).

6. HYDRODINAMIC RECONSTRUCTION AND HAZARD PATTERN EVALUATION

6.1. Hydraulic simulation and wood clogging

Considering the range 105-140 m^3/s, the hydraulic simulation of the event was carried out iteratively in a selected control reach (a few meters upstream of section 5 to a few meters downstream of section 6 using the step-backwater method.

The bed in this reach satisfies basic hydraulic criteria for discharge estimation, guaranteeing that changes in channel geometry were minimal after this flood event. The model applied was the one dimensional step-backwater program HEC-RAS 4.1 (USACE, 2010b) in permanent conditions.

The reach geometry (length 200 m, altitude range 805 - 755 m.a.s.l.) was produced using a combination of differential GPS and Total Station (cross section 10 m maximum spacing). The bridge structure was mapped more precisely. This detailed survey also allowed improvements to the available DEM, (5 m pixel size), and the more accurate DEM (0.65 m pixel size) was used for further spatial analysis with ArcGIS 9.3, ESRI, 2010) and the HEC-GeoRAS 4.3.93 tool (USACE, 2011).

The Manning roughness coefficient was established with aerial orthophotos from 2000 to 2010, and taking into account the evolution of the vegetation within the stream in order to assess the correct values for the vegetation stand in 1997. This roughness coefficient was established on both banks and riverbed for each cross section. Values ranged from 0.03 $m^{1/2}$ s^{-1} to 0.06 $m^{1/2}$ s^{-1} on low or non-vegetated banks; from 0.08 $m^{1/2}$ s^{-1} to 0.15 $m^{1/2}$ s^{-1} on vegetated banks; and from 0.08 $m^{1/2}$ s^{-1} to 0.1 $m^{1/2}$ s^{-1} in the main channel (higher values where large boulders were present).

Then, trial and error discharges (ranging from 10 to 200 m^3 s^{-1}) were entered into the model varying the geometry of the bridge section. This was carried out reducing the cross sectional area of the by 10% each time in an iterative procedure using the multiple block obstruction tool; this obtained the ratio between the percentage of occlusion and the water level for a given discharge, or *clogging curves* (Figure 6).

Figure 6: *(A) Clogging curves: water depth in section 6 represented on the Y-axis, and the reduced area in the bridge section in percentage on the X-axis. (B) Three types of behaviour can be differentiated in the curves: LT, CT and UT (explained in the text).*

It can be seen that for the proposed discharge range 105-140 m^3 s^{-1} a reduction from 40 to 56 % (48 ± 8 %) is required to reach the estimated water level. Lower discharge values, would need more than 60 % obstruction. On the other hand, with higher discharges the water level is reached almost without obstruction.

Figure 6 shows three different regions, corresponding to three different types of behaviour that can be observed in the clogging curves. The first region is the lower threshold (LT), where the slight water level increase is apparently linear when the clogging percentage increases (subparallel curves). The second region, critical threshold

(CT) shows the most significant behaviour, where small increments in clogging percentage make the water level rises rapidly, until the upper threshold (UT) or third region is reached, where the maximum water level remains almost constant.

6.2. Influence of wood clogging in flash flood hazard patterns

Other results obtained from the hydraulic simulation were the flooded area and water depth for the estimated peak discharge (central value of 123 m^3/s). The simulation was run with and without any bridge obstruction (Figure 7 shows the longitudinal sections and cross section of the bridge and figure 8 shows the maps).

Figure 7: *Results from the hydraulic simulation (123 m3 s^{-1} peak discharge). Longitudinal sections of the bridge reach with obstruction in the bridge (A) and without obstruction (B). (C) Bridge sketch.*

Figure 8*: Water depth for the estimated discharge of the 1997 flash flood, (A) without any obstruction in the bridge, (B) taking into account the LWD and the obstruction in the bridge, (C) flooded area with LWD (in red) and without LWD (blue).Gas deposits and camping site are shown on the maps.*

Figure 8 shows clearly that the flooded areas are probably different in the absence of wood. This suggests that specific areas will flood more frequently than expected if large woody debris is presented. The next step, therefore, was to analyse the flash flood frequency in the study area. To attempt to assign a return period value to the 1997 peak flow, data obtained from the Centro de Estudios Hidrográficos (CEDEX) regional study of maximum discharges (CEDEX, 2011; Spanish Ministery of Public Works) was

examined in this regional study of maximum discharges. In this study, frequency analyses of catchments smaller than 50 km^2 are carried out using the rational method. According to these, (the frequency curve is represented in Figure 8 as a continuous black line) the return period of the 1997 event is 80 - 200 years (depending on the range 123 ± 18 m^3 s^{-1}). However, if the authors' own short recorded data series is computed within the catchment with the estimated discharge for the 1997 event, and adjusted using different frequency distributions (GEV, Gumbel and LogPearson III; Figure 6, dotted grey lines) different results are obtained. For the 1997 event the recurrence time would range from 25 - 45 years (depending on the range 123 ± 18 m^3 s^{-1}). This is consistent with the observations made by Ballesteros et al., (2010 a and b) on the average age of the riparian vegetation (this could be related to another event that strongly damaged the vegetation).

For higher discharges the uncertainty increases due to the short data series. But the most important observation is that these curves are all above the other curve shown, so that the frequency may be underestimated.

Figure 9: *in the Arroyo Cabrera catchment. Continuous black line shows frequency distribution of CEDEX data. Dotted grey lines are the different adjustments using other frequency distributions; continuous grey line is the mean of these and the dashed area shows the confidence intervals (5 and 95%).*

In conclusion, the 1997 estimated discharge would have a return period of ~35±10 years (based on the mean of our approximations), however the wood clogging makes its consequences equivalent in water level and extension to a higher magnitude event (~100 year event). This hypothesis introduces the concept of the *equivalent return period,*

used here as the recurrence interval for an event of a given magnitude that in the presence of an obstruction (in this case wood, but it can be other) is equivalent in water level and flooded extension to an event without obstruction but of greater magnitude. An iterative process was carried out again to analyse this, and the results allowed the curves showing the defined equivalent return period to be computed (the curve estimated with the authors' recorded data and the one obtained from CEDEX, (2011) data, and the percentage of bridge obstruction (Figure 10).

***Figure 10**: Curve representing the effect of wood clogging in critical sections in flood hazard analysis. The broken red line is the estimated return period for the 1997 event based on the recorded short data series; the continuous blue line is the return period provided by CEDEX. The dotted black line is the mean and the grey shading shows the uncertainty area.*

Figure 10 shows that the 35 years return time event without any obstruction could be equivalent to the 50 years event if the cross sectional area would be reduced in a 50% and so on. Therefore, the discharge without obstruction increases the magnitude of its effects up to eight times depending on increasing obstruction.

7. DISCUSSION AND CONCLUSIONS

There are five main observations in this paper to be highlighted and discussed:

1. The discharge estimation 123 ± 18 $m^3 s^{-1}$ (7.94 ± 1.16 $m^3 s^{-1} km^{-2}$) was carried out first by means of empirical equations. The application of palaeocompetence equations to velocity reconstruction ideally requires assumptions about flow conditions to be met (steady, uniform flow, logarithmic velocity profiles and fully submerged particles with low relative roughness values) according to Costa, (1983) and Maizels, (1983). Although these assumptions can be questioned for a mountain flood and should be treated with caution, this approach allowed the discharge order of magnitude to be obtained, and was the first step towards the hydraulic simulation and reconstruction of the complex clogging process. These estimations are also consistent with a previous study of the site (Ballesteros et al., 2011).

2. Because there were only 10 daily rain gauges irregularly distributed in the study area in 1997, secondary information was used with the altitude obtained from a DEM as an easy-to-measure variable, with complete coverage of the study area and correlated with rainfall. The advantages of using the DEM together with rain gauge data in estimating daily rainfall have been shown (Pardo-Igúzquiza, 1998; Goovaerts, 2000). The same is true when generating geostatistical simulations of daily rainfall.

Stochastic simulations provide description and measurement of the uncertainty of the spatial variability of a phenomenon (Remy et al., 2009). This is done by generating multiple realizations of the stochastic process modelling the spatial distribution under study. The 500 simulations of data from these 10 stations provided 58 reliable realizations that satisfied the imposed conditions for the study site and the studied event.

3. The HEC-HMS rainfall-runoff model has also been applied in the past for various purposes (Scharffenberg and Fleming, 2005; Fleming and Neary, 2004; Maskey

et al., 2004; Cunderlik and Simonovic, 2007). The inverse hydrological problem has been solved to analyze the possible rainfall field configuration and duration. The desegregation applying different hyetotypes allowed different hydrological responses to be observed, to find the most reliable hyetograph, storm duration, precipitation amount and maximum intensities required to produce the estimated discharge. The simulations showed that a 12 hour storm, triangular increasing rate and isosceles triangular rate hyetographs, with simulated maximum rainfall intensities ranged from 25 to 4 mm h^{-1} and mean precipitation over the catchment ranging from 205 to 260 mm reproduce the catchment response during the 1997 event. These results agree with previous estimations based on landslide triggering precipitation threshold occurring in 1997 (Ruiz-Villanueva et al., 2011).

4. The hydraulic simulation has been carried out using the model HEC-RAS. This model has very often been used successfully to reconstruct past floods (some examples are Agget and Wilson, 2009; Balasch et al., 2010; Benito et al., 2003a and b; Gül et al., 2009; Horrit and Bates, 2002; Jacoby et al., 2008; Koutroulis and Tsanis., 2010; Ortega and Garzón, 2009; Seidel et al., 2009; Thorndycraft et al., 2005).

The Manning coefficient is considered to be of low sensitivity when calculating flow discharges of high magnitude floods (O'Connor and Webb, 1988; Enzel et al., 1994) showing that a 20 % change in this parameter produced a change of less than 5 % in the corresponding discharge.

In this study this model allowed the bridge structure and the cross sectional reduction to be accurately simulated (using the multiple block obstruction tool), and also the flooded area and water level.

5. According to Sear et al., (2010) wood dynamics may influence flooding frequency, extent and duration. This is exactly the case here. The blockage of the bridge during the flood due to the woody material generated flow interferences. The most important outcome was the increased water level upstream. This process had a considerable impact on increased risk as shown in detail above. Clogging curves have been developed for the study site and the concept of equivalent return period has been established. These important contributions enabled improved risk analysis taking this process into account. Three types of behaviour were observed in the clogging curves: the lower threshold where the slight increase in water level is linear when the clogging percentage increases; the critical and most important threshold, where small increments in clogging percentage make the water level rise rapidly, until the upper threshold is reached, where the maximum water level remains almost constant.

These behaviours can be explained by flow regime changes. First, in the region LT the flow regime is supercritical, and the water level increases apparently linearly (sub parallel curves) with the obstruction increases; then, the regimen changes into subcritical, and the water level increases abruptly (CT). Last, in UT region,(higher discharges and/or total obstruction) the wetted perimeter is increasing very slow, then the curve slope is less steeper than in the first region.

The *equivalent return period* is defined as the recurrence interval for an event of a given magnitude that in the presence of obstacles corresponds to an event which in absence of obstacles would have the same magnitude. On the study site the peak discharge without bridge obstruction increases its magnitude up to eight times in magnitude depending on the increase in obstruction.

The reconstruction of these past events will provide a better understanding of the catchment response and they will also improve risks analysis. The order of magnitude estimation of precipitation and discharge, and the post-event evaluation showed that the magnitude of this event was seriously influenced by the large quantities of wood transported in the flow and how this affected critical sections like bridges. These observations highlight the need to improve the study of woody debris transport during floods.

The hydrodynamic simulation of this process is needed to evaluate reliable scenarios and re-calculate the effects in terms of magnitude. Work is underway on this task (Ruiz-Villanueva et al., 2011 Abstract Floods3D; Ruiz-Villanueva et al., in preparation).

Finally, the concept of the equivalent return period may help to understand the influence of this (and other processes) in the flood hazard and risk analysis.

Acknowledgements

The authors want to express their gratitude to the Spanish Ministry of Science and Innovation, for financial support. This work was founded by CICYT MAS Dendro-Avenidas project (CGL2010-19274) and the Geological Survey of Spain (IGME). We are grateful to the Tagus Water Authority, Environment Department of Castilla y León in Ávila, Caja Ávila, Asocio de Ávila and Navaluenga Council for their collaboration. We want to address our special thanks to forester José Luis Galán for his assistance in the field. Furthermore we would like to enhance the contributions of Juan Ballesteros, Ignacio Gutierrez, Tasio Fernández, Leticia Salas, Carolina Guardiola and Ángel Prieto for their collaboration and interesting discussions and suggestions which significantly improved this paper.

REFERENCES:

Aggett GR, Wilson JP. 2009. Creating and coupling a high-resolution DTM with a 1-D hydraulic model in a GIS for scenario-based assessment of avulsion hazard in a gravel-bed river. *Geomorphology* **113***:* 21-34. DOI: 10.1016/j.geomorph.2009.06.034.

Andreoli A, Comiti F, Lenzi MA. 2007. Characteristics, distribution and geomorphic role of large woody debris in a mountain stream of the Chilean Andes. *Earth Surf. Process. Landforms* **32**, 1675–1692. DOI:10.1002/esp

Baker VR. 1984. Flood Sedimentation in Bedrock Fluvial Systems. In: *Sedimentology of gravels and conglomerates,* Koster, E.H., Steel, R.J. (eds.). Canadian Society of Petroleum Geologists Memoir **10**: 87–98.

Balasch JC, Ruiz-Bellet JL, Tuset J, Martín de Oliva J. 2010. Reconstruction of the 1874 *Santa Tecla*'s rainstorm in Western Catalonia (NE Spain) from flood marks and historical accounts. *Natural Hazards and Earth System Science*, **10**: 2317-2325. DOI:10.5194/nhess-10-2317-2010.

Ballesteros JA, Eguíbar M, Bodoque JM, Díez-Herrero A, Stoffel M, Gutiérrez-Pérez I. 2011. Estimating flash flood discharge in an ungauged mountain catchment with 2D hydraulic models and dendrogeomorphic paleostage indicators. *Hydrol. Process*. **25**: 970–979.

Ballesteros JA, Stoffel M, Bodoque JM, Bollschweiler M, Hitz O, Díez-Herrero A. 2010a. Changes in wood anatomy in tree rings of Pinus pinaster Ait. Following wounding by flash floods. *Tree-Ring Res*. **66:** 93–103.

Ballesteros JA, Stoffel M, Bollschweiler M, Bodoque JM, Díez-Herrero A. 2010b. Flash-flood impacts cause changes in wood anatomy of Alnus glutinosa, Fraxinus angustifolia and Quercus pyrenaica. *Tree Physiol*. **30**: 773–781.

Benito G, Díez-Herrero A, Fernandez de Villalata M. 2003. Magnitude and frequency of flooding in the Tagus basin (Central Spain) over the last millennium. *Climatic Change* **58**: 171–192.

Bocchiola D, Catalano F, Menduni G, Passoni G. 2002. An analytical–numerical approach to the hydraulics of floating debris in river channels. *Journal of Hydrology* **269**: 65-78. DOI:10.1016/S0022-1694(02)00195-6.

Bodoque JM, Eguibar MA, Díez-Herrero A, Gutiérrez-Pérez I, Ruiz-Villanueva V. 2011. Can the discharge of a past hyperconcentrated flow be estimated based on palaeoflood evidence?. *Water Resources Research*. Accepted for publication.

606 Borga M, Gaume E, Creutin JD, Marchi L. 2008. Surveying flash floods: gauging the
607 ungauged extremes. *Hydrological Processes* **22**: 3883-3885.
608 DOI:10.1002/hyp.7111
609 Braudrick C, Grant GE. 2000. When do logs move in rivers? *Water Resources Research*
610 **36:** 571. DOI:10.1029/1999WR900290.
611 Braudrick CA, Grant GE, Northwest P, Forest US. 2001. Transport and deposition of
612 large woody debris in streams□: a flume experiment. *Geomorphology* **41:** 263-
613 283.
614 Buxton TH. 2010. Modeling entrainment of waterlogged large wood in stream channels.
615 *Water Resources Research* **46**. DOI:10.1029/2009WR008041.
616 Camarasa AM, Tilford KA. 2002. Rainfall-runoff modelling of ephemeral streams in
617 the Valencia region (eastern Spain). *Hydrological Processes* **16**: 3329-3344.
618 DOI:10.1002/hyp.1103.
619 CEDEX 2011. Mapa de caudales máximos. Memoria tecnica.
620 http://www.marm.es/es/agua/temas/gestion-de-los-riesgos-de-
621 inundacion/memoria_tecnica_v2.0_tcm7-162773.pdf
622 Comiti F, Andreoli A, Mao L, Lenzi MA. 2007. Wood storage in three mountain
623 streams of the Southern Andes and its hydro-morphological effects. *Earth Surf.*
624 *Process. Landforms* **32:** 1675–1692. DOI:10.1002/esp.
625 Comiti F, Mao L, Preciso E, Picco L, Marchi L, Borga M. 2008. Large wood and flash
626 floods: evidence from the 2007 event in the Davča basin (Slovenia). *Monitoring,*
627 *Simulation, Prevention and Remediation of Dense Debris Flows II* **60**: 173-182.
628 DOI:10.2495/DEB080181.
629 Comiti F, Mao L, Wilcox A, Wohl E, Lenzi M. 2007. Field-derived relationships for
630 flow velocity and resistance in high-gradient streams. *Journal of Hydrology*,
631 **340**: 48-62. DOI:10.1016/j.jhydrol.2007.03.021.
632 Costa JE. 1983. Paleohydraulic reconstruction of flash-flood peaks fromboulder
633 deposits in the Colorado Front Range. *Geological Society of America Bulletin*
634 **94**: 986–1004.
635 Cunderlik JM, Simonovic SP. 2007. Inverse flood risk modelling under changing
636 climatic conditions. *Hydrological Processes* **21**: 563-577.
637 Diehl TH. 1997. Potential Drift Accumulation at Bridges. Publication No. FHWA-RD-
638 97-028.U.S.Department of Transportation, Federal Highway Administration
639 Research and Development, Turner-Fair- bank Highway Research Center,

Virginia. On the web at: http:// www.tn.water.usgs.gov/pubs/FHWA-RD-97-028/drfront1.htm.

Díez-Herrero A. 2003. Geomorfología e Hidrología fluvial del río Alberche. Modelos y SIG para la gestión de riberas. *Serie Tesis Doctorales 2. Publicaciones del Instituto Geológico y Minero de España (Ministerio de Ciencia y Tecnología, Madrid*. 587 pp.

Enzel Y, Ely LL, House PK, Baker VR, Webb RH. 1993. Palaeoflood evidence for a natural upper bound to flood magnitudes in the Colorado River basin. *Water Resour. Res*. **29:** 2287–2297.

Fleming M, Neary V. 2004. Continuous hydrologic modeling study with the Hydrologic Modeling System. *Journal of Hydrologic Engineering* **9/3**: 175-183.

Goovaerts P. 2000. Geostatistical approaches for incorporating elevation into the spatial interpolation of rainfall. *Journal of Hydrology*, **228**: 113-129.

Grimes D, Pardo-Igúzquiza E. 2010. Geostatistical analysis of rainfall. *Geographical Analysis* **42**: 136-160.

Gül GO, Harmancıoğlu N, Gül A. 2009. A combined hydrologic and hydraulic modeling approach for testing efficiency of structural flood control measures. *Natural Hazards* **54:** 245-260. DOI:10.1007/s11069-009-9464-2.

Haga H. 2002. Transport and retention of coarse woody debris in mountain streams: An in situ field experiment of log transport and a field survey of coarse woody debris distribution. *Water Resources Research* **38**. DOI:10.1029/2001WR001123.

Horritt M, Bates P. 2002. Evaluation of 1D and 2D numerical models for predicting river flood inundation. *Journal of Hydrology* **268**: 87-99. DOI:10.1016/S0022-1694(02)00121-X.

Hupp CR, Bornette G. 2003. Vegetation and fluvial processes and forms in temperate areas. In: *Tools in Fluvial Geomorphology*. Kondolf GM, Piegay H. (eds.). Chichester. J. Wiley & Sons: 269–288.

Jacoby Y, Grodek T, Enzel Y, Porat N, McDonald EV, Dahan O. 2008. Late Holocene upper bounds of flood magnitudes and twentieth century large floods in the ungauged, hyperarid alluvial Nahal Arava, Israel. *Geomorphology* **95**: 274-294. DOI:10.1016/j.geomorph.2007.06.008.

Johnson SL, Swanson FJ, Grant GE, Wondzell SM. 2000. Riparian forest disturbances by a mountain flood□? the influence of floated wood. *Hydrological Processes*,

14: 3031-3050. DOI:10.1002/1099-1085(200011/12)14:16/17<3031:AID-HYP133>3.0.CO;2-6.

Johnson RM, Warburton J. 2002. Flooding and geomorphic impacts in a mountain torrent: Raise Beck, central Lake District, England. *Earth Surface Processes and Landforms* **27**: 945-969. DOI:10.1002/esp.386.

Kehew AE, Milewski A, Soliman F. 2010. Reconstructing an extreme flood from boulder transport and rainfall–runoff modelling: Wadi Isla, South Sinai, Egypt. *Global and Planetary Change* **70**: 64–75.

Koutroulis AG, Tsanis IK. 2010. A method for estimating flash flood peak discharge in a poorly gauged basin: Case study for the 13–14 January 1994 flood, Giofiros basin, Crete, Greece. *Journal of Hydrology* **385**: 150-164.

Mao L, Comiti F, Lenzi MA. 2010. Bedload Dynamics in Steep Mountain Rivers□: Insights from the Rio Cordon Experimental Station (Italian Alps). *Main*, 253-265.

Marchi L, Borga M, Preciso E, Sangati M, Gaume E, Bain V, Delrieu G, 2009. Comprehensive post-event survey of a flash flood in Western Slovenia□: observation strategy and lessons learned. *Hydrological Processes*, **3770**:3761-3770. DOI:10.1002/hyp.

Maskey S, Guinot V, Price RK. 2004. Treatment of precipitation uncertainty in rainfall-runoff modelling: a fuzzy set approach. *Adv. Water Res*. **27**: 889–898.

Mazzorana B, Comiti F, Volcan C, Scherer C. 2011. Determining flood hazard patterns through a combined stochastic–deterministic approach. *Natural Hazards*. DOI:10.1007/s11069-011-9755-2.

Mazzorana B, Hübl J, Zischg A, Largiader A. 2010. Modelling woody material transport and deposition in alpine rivers. *Natural Hazards* 425-449. DOI:10.1007/s11069-009-9492-y.

Montesarchio V, Lombardo F, Napolitano F. 2009. Rainfall thresholds and flood warning: an operative case study. *Natural Hazards and Earth System Science*, **9**: 135-144. DOI:10.5194/nhess-9-135-2009.

Montgomery D, Piegay H. 2003. Wood in rivers: interactions with channel morphology and processes. *Geomorphology* **51**: 1-5. DOI:10.1016/S0169-555X(02)00322-7.

Moulin B, Piegay H. 2004. Characteristics and temporal variability of large woody debris trapped in a reservoir on the River Rhone implications for river basin management. *River Research and Applications* **20**:79-97. DOI:10.1002/rra.724.

O'Connor JE, Webb RH. 1988. Hydraulic modelling for paleoflood analysis. In *Flood Geomorphology*, Baker VC, Kochel RC, Patton PC (eds). Jhon Wiley & Sons, Inc.: New York; 393–402.

Ortega JA, Garzón-Heydt G. 2009. Geomorphological and sedimentological analysis of flash-flood depositsThe case of the 1997 Rivillas flood (Spain). *Geomorphology*, **112**: 1-14. doi:10.1016/j.geomorph.2009.05.004.

Palacios D, Garcia R, Rubio V, Vigil R. 2003. Debris flows in a weathered granitic massif: Sierra de Gredos, Spain. *Catena* **51**: 115–140.

Palacios D, Marcos J, Vázquez-Selem L. 2011. Last glacial maximum and deglaciation of Sierra de Gredos, Central Iberian Peninsula. *Quaternary Internacional* **233**: 16–26.

Pardo-Igúzquiza E. 1998. Comparison of geostatistical methods for estimating the areal average climatological rainfall mean using information of precipitation and topography. *International Journal of Climatology* **18**:1031-1047.

Remy N, Boucher A, Wu J. 2009. Applied Geostatistics with SGeMS: A User's Guide. Cambridge University Press. 264pp.

Ruiz-Villanueva V, Bodoque JM, Díez-Herrero A, Calvo C. 2011. Triggering threshold precipitation and soil hydrological characteristics of shallow landslides in granitic landscapes. *Geomorphology* **133**: 178-189.

Ruiz-Villanueva V, Bladé-Castellet E, Sánchez-Juny M, Bodoque JM, Díez-Herrero A. 2011. Woody debris transport during floods: 2d hydrodynamic modelling approach. *Floods in 3d: processes, patterns, predictions. EGU 2011 Leonardo Conference.* Bratislava, Slovakia, 23-25 November 2011

Salas L, Fernandez T. 2007. "In-site" regionalization to estimate an intensity– duration–frequency law: a solution to scarce spatial data in Spain. *Hydrological Processes* **21**:3507–3513.

Scharffenberg WA, Fleming MJ. 2005. Hydrologic modelling system, HEC-HMS, User's Manual, 248 pp.

Sear DA, Millington CE, Kitts DR, Jeffries R. 2009. Logjam controls on channel:floodplain interactions in wooded catchments and their role in the formation of multi-channel patterns. *Geomorphology* **116**: 305–319.

Sivapalan M, Bloschl G, Zhang L, Vertessy R. 2003. Downward approach to hydrological prediction. *Hydrological Processes* 17: 2101–2111, DOI: 10·1002/hyp.1425.

Smith JA, Baeck ML, Ntelekos AA, Villarini G, Steiner M. 2011. Extreme rainfall and flooding from orographic thunderstorms in the central Appalachians, *Water Resour. Res.* **47**, W04514, doi:10.1029/2010WR010190.

Thorndycraft VR, Benito G, Rico M, Sopeña A, Sánchez Y, Casas A. 2005. A long-term flood discharge record derived from slackwater flood deposits of the Llobregat River, NE Spain. *J. Hydrol*. **313**:16–31.

US Army Corps of Engineers (USACE). 2009. HEC-HMS 3.5 User Manual, US Army Corps of Engineers Hydrologic Engineering Center, Davis, CA.

US Army Corps of Engineers (USACE). 2010a. HEC-GeoHMS 4.2 User Manual, US Army Corps of Engineers Hydrologic Engineering Center, Davis, CA.

US Army Corps of Engineers (USACE). 2010b. HEC-RAS River Analysis System: Hydraulic Reference Manual, US Army Corps of Engi- neers Hydrologic Engineering Center, Davis, CA.

US Army Corps of Engineers (USACE). 2011. HEC-GeoRAS Users Manual, US Army Corps of Engi- neers Hydrologic Engineering Center, Davis, CA.

Vélez JJ, López F, Puricelli M, Francés F. 2007. Parameter extrapolation to ungauged basins with a hydrological distributed model in a regional framework. *Hydrol. Earth Syst. Sci. Discuss*. **4:** 909–956.

Weingartner R, Barben M, Spreafico M. 2003. Floods in mountain areas—an overview based on examples from Switzerland. *Journal of Hydrology* **282**: 10-24. DOI:10.1016/S0022-1694(03)00249-X.

Wohl E, Bolton S, Cadol D, Comiti F, Goode JR, Mao L. 2011. A two end-member model of wood dynamics in headwater neotropical rivers. *Journal of Hydrology* 1-10. Elsevier B.V. doi:10.1016/j.jhydrol.2011.01.061.

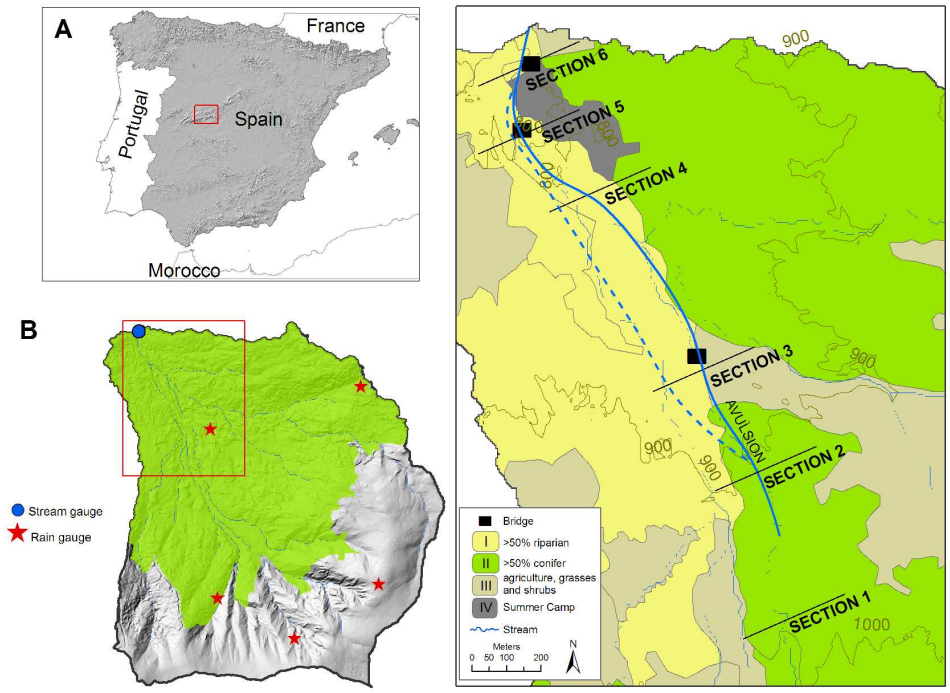

Figure 1
297x210mm (300 x 300 DPI)

	Values	Unit
Area	15.5	km^2
Minimum elevation	735	m a.s.l
Maximum elevation	1923	m a.s.l
Length of the main channel	5.5	km
Mean gradient of the main channel	21.6	%
Stream order	3	-
Mean annual precipitation (lowland)	554	mm
Mean annual precipitation (high altitude)	~2000	mm
Maximum water discharge recorded*	45.6	$m^3 s^{-1}$

*The value refers to the flow gauge installed since 2004.

***Table 1**: Main physical characteristics of the Arroyo Cabrera catchment.*

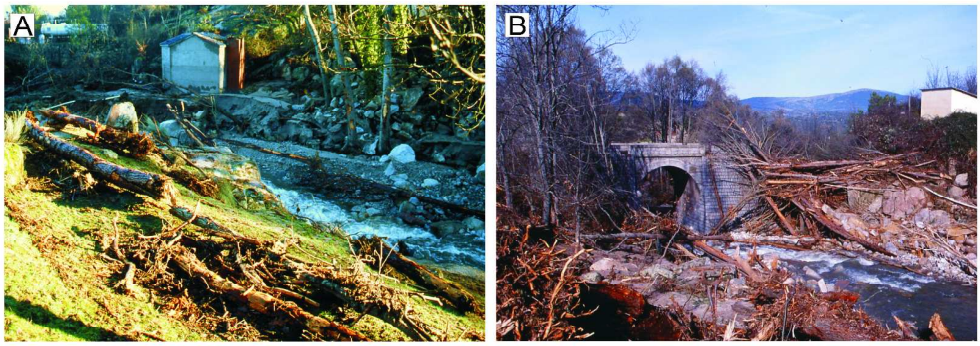

Figure 2
416x161mm (300 x 300 DPI)

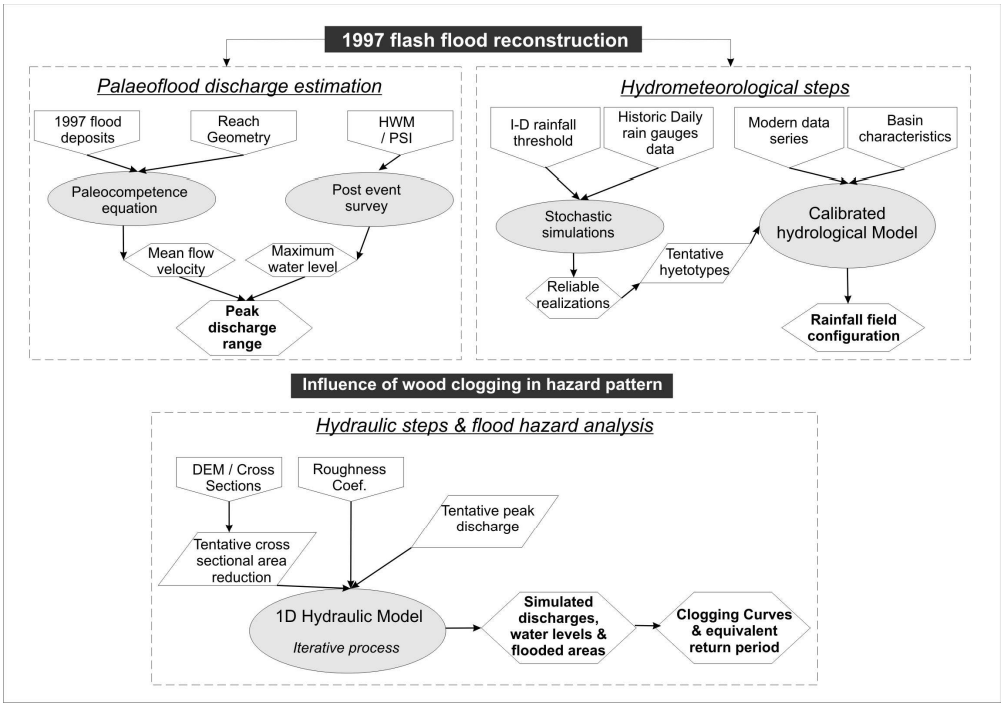

Figure 3
194x135mm (300 x 300 DPI)

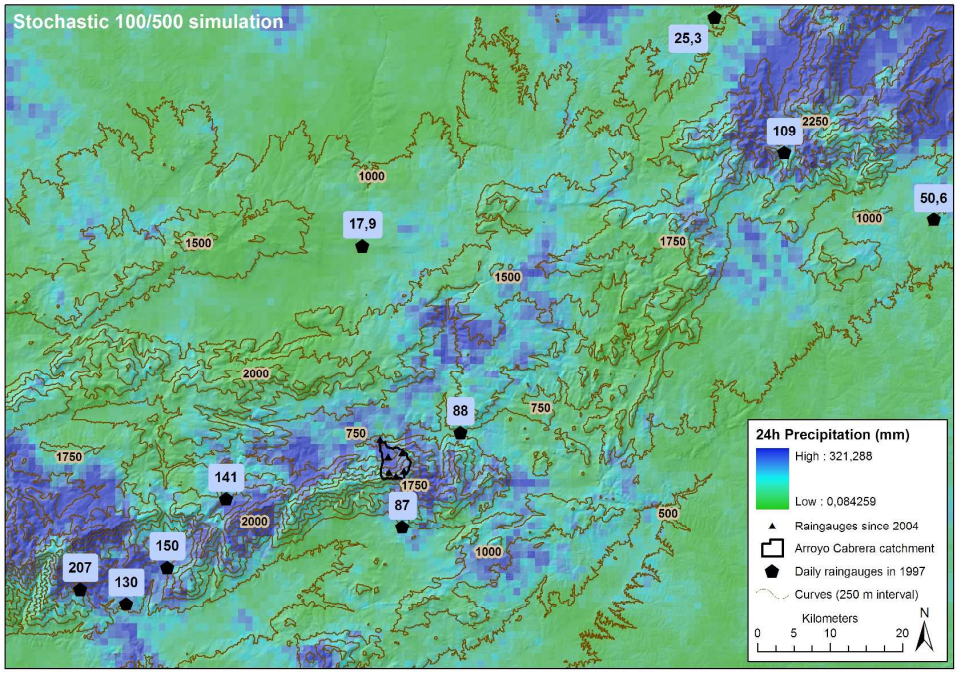

Figure 4
296x210mm (300 x 300 DPI)

Task	Methodology/Software
Generation of realizations of daily rainfall fields	Geostatistical conditional simulationa using sequential cokriging as implemented in the software SGeMS (Remy et al., 2009)
Selection of reliable realizations	ArcGis 9.3 (Spatial Analysis and Model Builder tools) (ESRI, 2010)
Basin and subbasins modelling	ArcGis 9.2, HEC-GeoHMS 4.2 and Hec HMS 3.5 (USACE, 2009 and 2010a
Transformation of excess precipitation to runoff	SCS dimensionless unit hydrograph method
Simulation of channel routing	Muskinghum-Cunge method
Simulation of baseflow	Recession method
Calibration of hydrologic model	Minimization of the sum of squared residuals
Temporal desegregation of daily rainfall: Intensity-duration curves	Equation proposed by Salas and Fernández, 2007 for Spain
Hyetotype models	Models used by Montescarchio et al., 2009.

***Table 2**: Summary of methods used in the Hydrometeorological reconstruction*

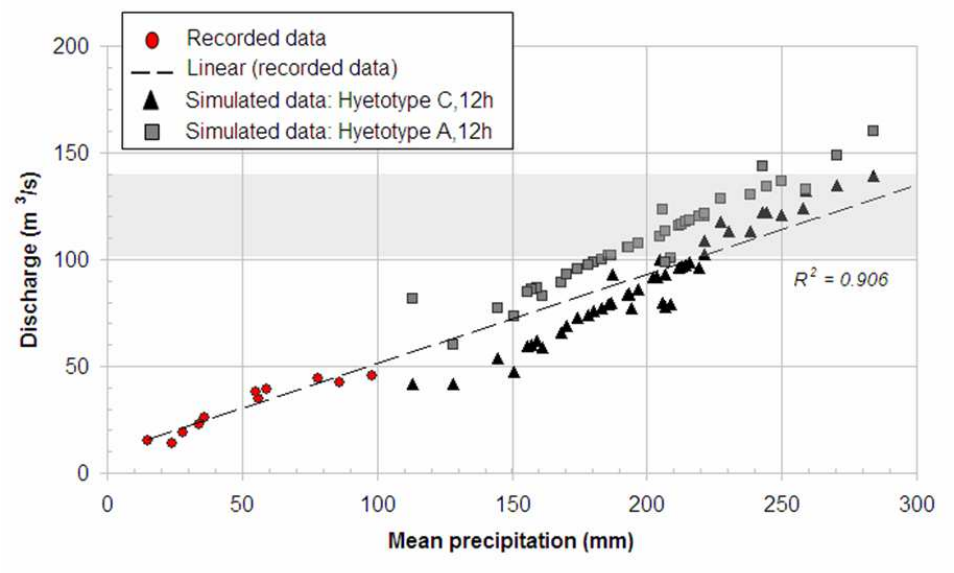

figure 5
254x190mm (96 x 96 DPI)

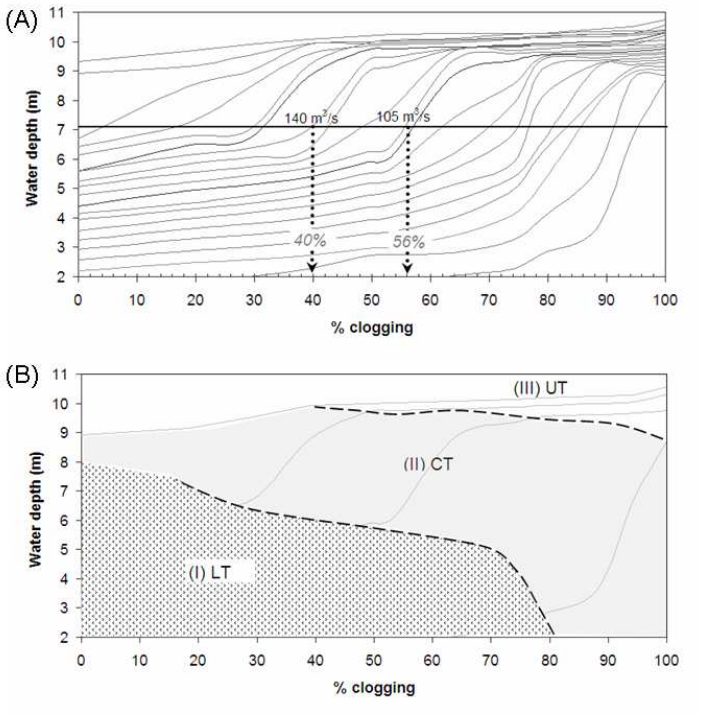

figure 6
254x190mm (96 x 96 DPI)

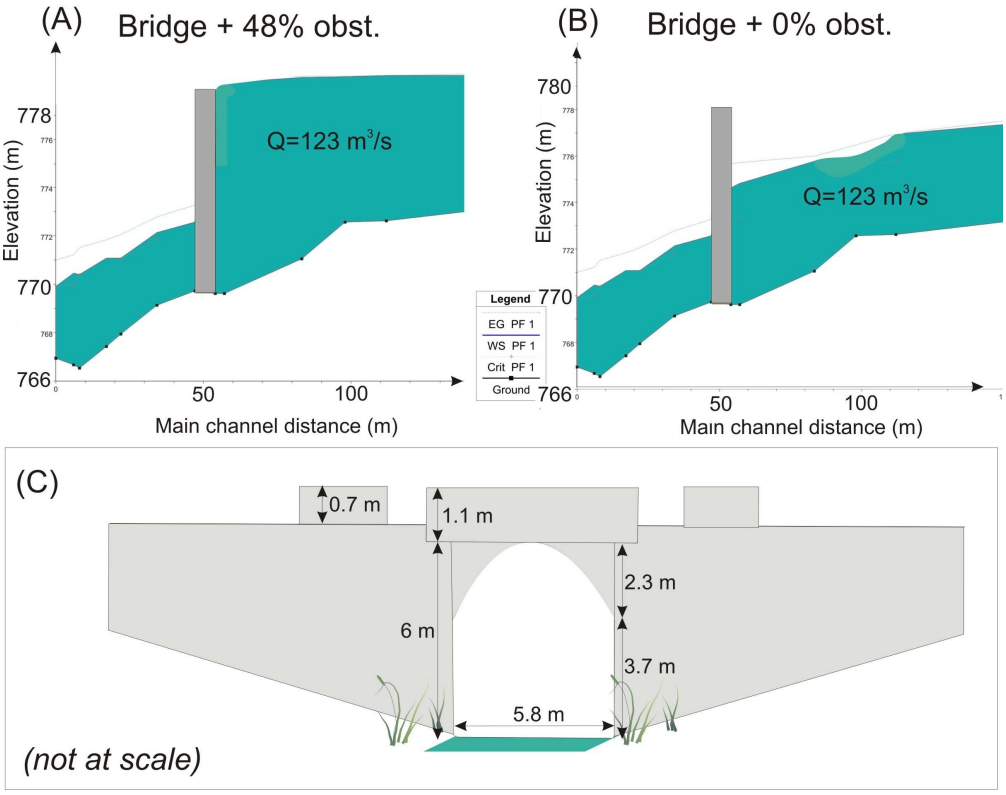

Figure 7
204x163mm (300 x 300 DPI)

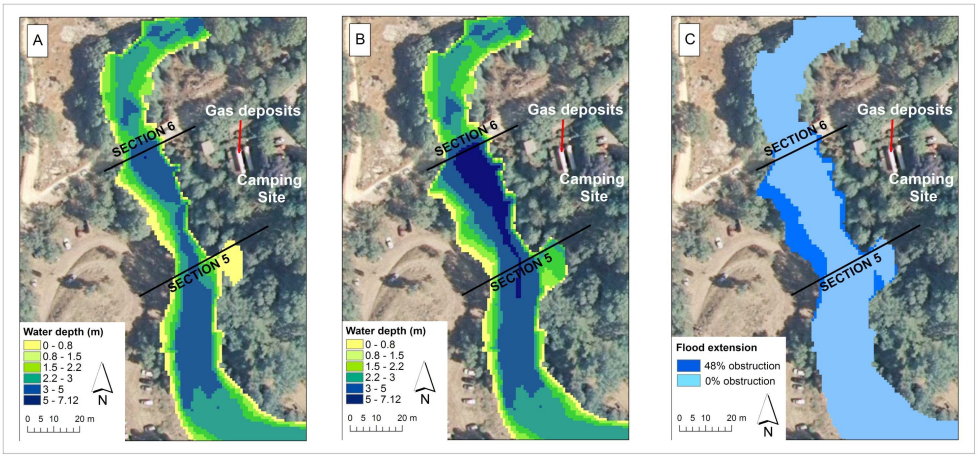

figure 8
257x125mm (300 x 300 DPI)

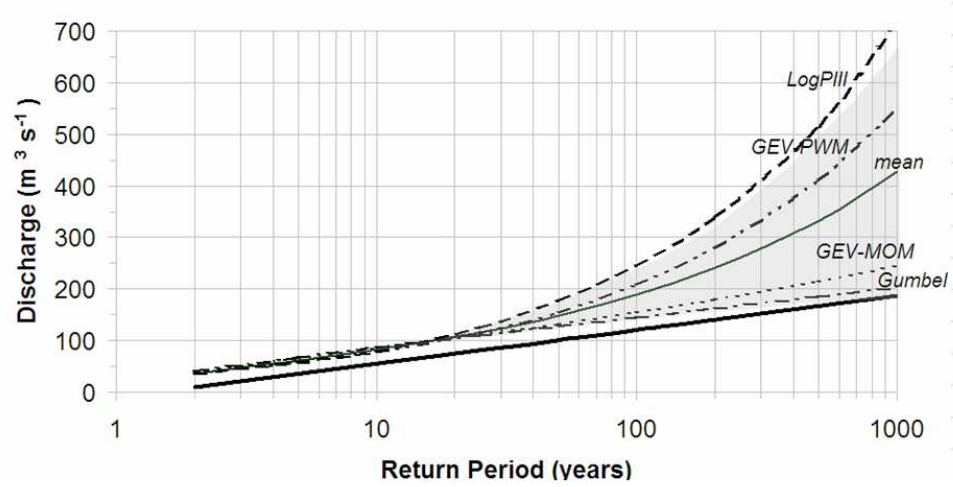

figure 9
254x190mm (96 x 96 DPI)

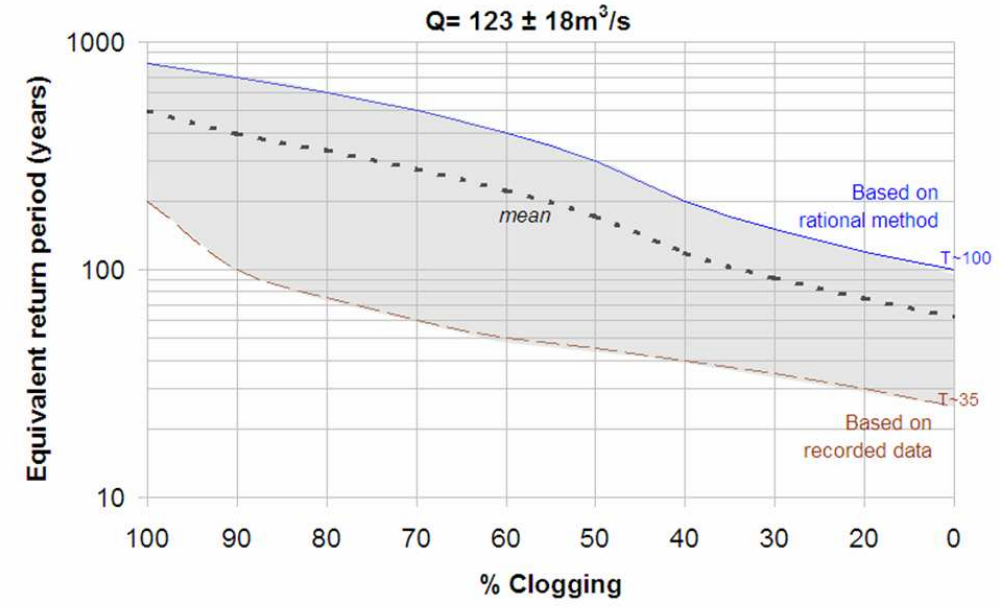

Figure 10
254x190mm (96 x 96 DPI)